Applied Physics B (2024) 130:161
https://doi.org/10.1007/s00340-024-08304-y

Applied Physics B
Lasers and Optics

RESEARCH

A high peak power and low peak-to-peak instability mid-infrared optical parametric oscillator pumped by a 1064 nm electro-optic cavity-dumped pulsed laser

Guozhen Wang[1] · Yang Bai[1,2] · Yi Li[3] · Shunyu Yang[1] · Xiaoying Zhang[3] · Wenrui Duan[3] · Baole Lu[1,2]

Received: 28 June 2024 / Accepted: 7 August 2024 / Published online: 20 August 2024

Abstract
In this paper, we demonstrate a tunable mid-infrared (mid-IR) optical parametric oscillator (OPO) using an MgO: PPLN crystal with a polarization period of 29.8 μm, which was end-pumped by a 1064 nm electro-optic cavity-dumped all-solid-state laser (1064 nm EOCD-laser) with a pulse repetition frequency range of 100 Hz to 1 kHz. Thanks to the use of 808 nm pulsed laser diode (LD) side-pumping Nd: YAG crystal, transverse electro-optic modulating (TEOM) MgO: LN crystal, and birefringent crystal (BC) filtering in the 1064 nm cavity-dumped cavity, both the 1064 nm EOCD-laser and the idler light output by the OPO exhibited high peak power and low peak-to-peak instability in both pulse width and single pulse energy. By combining temperature tuning of the MgO: PPLN crystal from 30 °C to 200 °C, wavelength tuning of the idler light from 3705.2 to 3424.3 nm was achieved. For the first time, a pulsed idler light at 3705.2 nm with a high peak power of 1.224 MW, a narrow pulse width of 4.97 ns, and an optical-to-optical (1064 nm to 3705.2 nm) conversion efficiency of 38.1% was obtained, corresponding to a tuning temperature of 30 °C and a pulse repetition frequency of 100 Hz. The peak-to-peak instability for both pulse width and single pulse energy was only ± 1.04% and ± 1.41%, respectively.

1 Introduction

The 3–5 μm mid-infrared (mid-IR) band is a well-known and important atmospheric window. Mid-IR lasers operating in this range offer excellent atmospheric penetration and feature rich molecular functional group absorption peaks, making them highly valuable for applications in atmospheric remote sensing, environmental monitoring, laser radar, and optoelectronic countermeasures [1–3]. Currently, various types of mid-IR lasers are available, including argon fluoride excimer lasers (DF lasers), quantum cascade lasers, frequency-doubled lasers, and optical parametric oscillators (OPOs) [4–7]. Among these, OPOs based on quasi-phase matching technology and pumped by 1064 nm pulsed laser beams have garnered significant attention due to their simple structure, high optical-to-optical conversion efficiency, and tunable wavelength.

In practice, peak power is a critical parameter that directly determines the maximum detection distance of 3–5 μm mid-IR pulsed OPOs. Higher peak power enhances the potential for achieving longer detection ranges [8, 9]. Additionally, the peak-to-peak instability of pulse width and single pulse energy is another critical parameter for assessing the output stability of mid-IR pulsed OPOs [10, 11]. To improve the detection accuracy of mid-IR pulsed OPOs, it is essential to further reduce the peak-to-peak instabilities of both pulse width and single pulse energy [12, 13]. Therefore, increasing peak power and minimizing peak-to-peak instability would improve both the detection range and accuracy of mid-IR pulsed OPOs in practical applications.

As one of the crucial components for 3–5 μm mid-IR pulsed OPOs, the technical specifications of the 1064 nm laser pump sources directly impact the output performance of the OPOs. Currently, 3–5 μm mid-IR pulsed OPOs primarily use all-solid-state lasers or fiber lasers operating in Q-switched or mode-locked configurations as pump sources. Multi-mode Q-switched 1064 nm lasers, which rely on

✉ Yang Bai
by@nwu.edu.cn

[1] Institute of Photonics & Photon-Technology, Northwest University, Xi'an 710127, China

[2] Shaanxi Engineering Technology Research Center for Solid State Lasers and Application, Xi'an 710127, Shaanxi, China

[3] Key Laboratory of Metrological Optics and Application for State Market Regulation, Shaanxi Institute of Metrology Science, Xi'an 710199, Shaanxi, China

energy storage in the upper level of the gain medium, can output nanosecond laser pulses [14–16]. However, effectively reducing the peak-to-peak instability of 1064 nm multi-mode Q-switched lasers is challenging due to adverse factors such as thermal relaxation oscillations in the gain medium, significant variations in pulse width with pulse repetition frequency and pump power, and mode hopping. In contrast, single-frequency Q-switched 1064 nm lasers are characterized by low peak-to-peak instabilities due to the absence of mode competition [17, 18]. However, it is often necessary to insert a high-loss Fabry–Perot etalon or a volume Bragg grating into the cavity. This insertion results in reduced output energy for the 1064 nm single-frequency Q-switched lasers. Typically, achieving high-energy laser pulses requires seed pulse amplification, which is technically complex and expensive. The 1064 nm mode-locked all-solid-state lasers or fiber lasers demonstrate characteristics such as minimal influence of pulse repetition frequency on pulse width and low peak-to-peak instabilities, among others [19–21]. However, adjusting the pulse repetition frequency of 1064 nm mode-locked lasers with a fixed cavity length and increasing its average and peak power presents a significant challenge. The above research results indicate that increasing the peak power of 1064 nm pump sources based on gain medium energy storage while reducing their peak-to-peak instability is a highly challenging research task.

It is worth noting that employing cavity dumping techniques based on intracavity photon storage can cause periodic variations in the polarization direction of the 1064 nm fundamental frequency laser. This allows the output rate of the 1064 nm laser cavity to change rapidly and periodically from 0 to 100% [22–24]. Compared to the conventional 1064 nm pumped sources mentioned above, the 1064 nm electro-optic cavity-dumped all-solid-state laser (1064 nm EOCD-laser) offers several advantages. These include intracavity photon storage, which effectively reduces thermal effects in the gain medium, a high-quality resonant cavity, and a pulse width determined solely by the cavity length and the rise response time of the high-voltage electric field applied to the electro-optic crystal switch [25–27]. These advantages contribute to obtaining high peak power and low peak-to-peak instability of the pulse width and single pulse energy in the 1064 nm EOCD-laser output. Additionally, employing birefringent crystal (BC) filtering on the 1064 nm fundamental frequency light to reduce its number of longitudinal modes and lower its noise has been proven to be effective [28, 29]. However, there have been few reports dedicated to the 3–5 μm mid-infrared pulsed OPOs with high peak power and low peak-to-peak instability, using a 1064 nm EOCD-laser with BC filtering as the pump source.

In this paper, we present a mid-infrared pulsed OPO using a 1064 nm EOCD-laser with BC filtering as the pump source. This setup achieves high peak power and low peak-to-peak instability in both pulse width and single pulse energy. The 1064 nm EOCD-laser is based on 808 nm pulsed laser diode (LD) side-pumping Nd: YAG crystal rod, transverse electro-optic modulated (TEOM) magnesium-oxide-doped lithium niobate (MgO: LN) crystal, and BC filtering. A magnesium-oxide-doped periodically poled lithium niobate (MgO: PPLN) crystal with a poling period of 29.8 μm in a mid-IR pulsed OPO cavity is end-pumped from the 1064 nm EOCD-laser. In the temperature tuning range of 30 °C to 200 °C for the MgO: PPLN crystal, a mid-IR pulsed idler light with a wavelength tuning range of 3705.2 nm to 3424.3 nm and a pulse repetition frequency tuning range of 100 Hz to 1 kHz was obtained. At the maximum LD pump current of 75 A and the minimum tuning temperature of 30 °C, the average power of the mid-IR pulsed idler light corresponding to a wavelength of 3705.2 nm ranged between 0.61 W at 100 Hz to 2.54 W at 1 kHz, with pulse width consistently less than 6 ns, and peak powers between 1.22 MW at 100 Hz to 0.43 MW at 1 kHz. The peak-to-peak instability of the pulse width and single pulse energy increased from ± 1.04% at 100 Hz to ± 1.52% at 1 kHz and from ± 1.41% at 100 Hz to ± 2.01% at 1 kHz, respectively.

2 Experimental setup

A mid-IR pulsed OPO using a 1064 nm EOCD-laser with BC filtering as the pump source was designed, as shown in Fig. 1. Among them, the cavity of the 1064 nm EOCD-laser was composed of a mirror M_1, a water-cooled Nd: YAG module, a Brewster plate-1 (BP_1), a BC, a TEOM-MgO: LN crystal, a Brewster plate-2 (BP_2), and a mirror M_2. In the water-cooled Nd: YAG module, a 1.0 at.% Nd^{3+}-doped Nd: YAG crystal rod (diameter of 2 mm, length of 50 mm) as a gain medium was side-pumped by three 808 nm pulsed LD arrays. Three LD arrays were distributed in an angle of 120° mutually. The pulse repetition frequency range, pulse width, maximum pumping current, and pump duty ratio of the three 808 nm pulse LD arrays were 100 Hz to 1 kHz, 200 μs, 75 A, and 25%, respectively. Compared to the traditional longitudinal voltage application mode, the transverse voltage application mode can effectively reduce the half-wave voltage of electro-optic crystals, decrease the risk of high voltage breakdown, and shorten the switching time [30]. This approach is beneficial for compressing the pulse width of the pulsed laser and reducing its peak-to-peak instability. A 6.0 mol.% MgO-doped TEOM-MgO: LN crystal with dimensions of 3 mm × 7 mm × 20 mm and an optical damage threshold of 200 MW/cm^2 (with a spacing of 3 mm between the positive and negative electrodes) was used due to the considerations of low transverse half-wave voltages, resistance to deliquescence, and low cost. The TEOM-MgO:

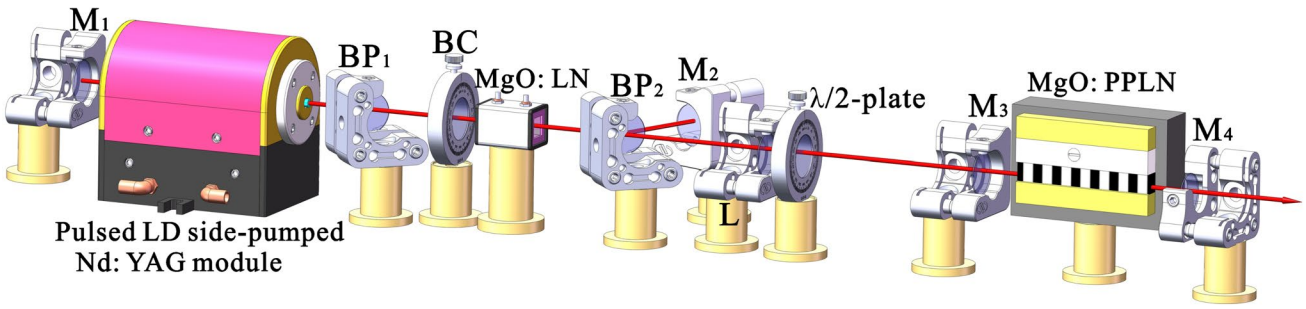

Fig. 1 Experimental setup for OPO pumped by a 1064 nm EOCD-laser

LN crystal was driven by a high-voltage power supply with a rising- and falling-edge response time of about 4 ns @ 10 Hz, a modulation frequency range of 1 Hz to 2 kHz, and a half-wave voltage of about 3.5 ± 0.2 kV @ 1064 nm. To achieve high reflection of s-polarized light and high transmission of p-polarized light in the cavity, the normal lines to the incident planes of the BP_1 and BP_2 with both thickness of 2 mm, were aligned at a Brewster angle of 55.6° relative to the optical axis of the linear cavity. A synchronous signal generator was used to ensure that the LD arrays and the TEOM-MgO: LN crystal could be triggered synchronously.

As shown in Fig. 1, the un-polarized 1064 nm fundamental frequency light generated by the stimulated emission from the Nd: YAG crystal changes into a partially polarized light dominated by p-polarization state and containing a small amount of s-polarization state after passing BP_1 placed at Brewster angle. When the optical axis of the p-polarized 1064 nm fundamental frequency light transmitted through the BP_1 forms a 45° angle with the optical axis of the 2.4 mm thick BC (quartz crystal), the polarization state of the p-polarized 1064 nm fundamental frequency light remains unchanged after a single round trip through the BC.

When the transverse half-wave voltage is applied to the TEOM-MgO: LN crystal, the p-polarized 1064 nm fundamental frequency light is converted to s-polarized fundamental frequency light after a single pass through the TEOM-MgO: LN crystal. The s-polarized 1064 nm fundamental frequency light is then successively reflected by the BP_2 and M_2. Upon passing through the TEOM-MgO: LN crystal again, its polarization state is converted back to p-polarized. At this point, the oscillation and amplification of p-polarized 1064 nm fundamental light with zero output rate and the energy storage in the form of photons are realized in the cavity. Conversely, a small amount of the s-polarized 1064 nm fundamental frequency light is converted to p-polarized fundamental frequency light after a single pass through the TEOM-MgO: LN crystal. The converted p-polarized 1064 nm fundamental frequency light will pass directly through BP_2 and exit the cavity, thereby preventing it from oscillating in the cavity. When the half-wave voltage applied to the TEOM-MgO: LN crystal is removed, the photon energy that has undergone a single round-trip

Table 1 Coating on the surfaces of the optical element (*R*: reflectivity)

Optical element	Incident surface	Output surface
Nd: YAG	$R < 0.3\%$ @1064 nm at 0°	$R < 0.3\%$ @1064 nm at 0°
M_1	$R > 99.7\%$ @1064 nm at 0°	No
BP_1	$R < 0.3\%$@1064 nm at 55.6°	$R < 0.3\%$@1064 nm at 55.6°
MgO: LN	$R < 0.3\%$ @1064 nm at 0°	$R < 0.3\%$ @1064 nm at 0°
BC	$R < 0.3\%$@1064 nm at 0°	$R < 0.3\%$@1064 nm at 0°
BP_2	$R < 0.3\%$@1064 nm at 55.6°	$R < 0.3\%$@1064 nm at 55.6°
M_3	$R < 0.3\%$@1064 nm at 0°	$R < 1.0\%$@1064 nm + $R > 99.2\%$ @1460—1700 nm + $R > 95.0\%$ @3400—3750 nm at 0°
MgO: PPLN	$R < 1.0\%$@1064 nm + $R < 1.0\%$@1460—1700 nm + $R < 5.0\%$ @3400—3750 nm at 0°	$R < 1.0\%$@1064 nm + $R < 1.0\%$@1460—1700 nm + $R < 5.0\%$ @3400—3750 nm at 0°
M_4	$R > 99.2\%$ @1460—1700 nm + $R < 5.0\%$ @3400—3750 nm at 0°	$R < 1.0\%$ @3400—3750 nm at 0°
L	$R < 0.3\%$@1064 nm at 0°	$R < 0.3\%$@1064 nm at 0°
λ/2 plate	$R < 0.3\%$@1064 nm at 0°	$R < 0.3\%$@1064 nm at 0°

in the cavity is fully extracted through BP_2, resulting in a p-polarized 1064 nm laser pulse.

The OPO cavity was composed of a mirror M_3, a MgO: PPLN crystal, and a mirror M_4. The 6.0 mol.% MgO-doped MgO: PPLN crystal with a polarization period of 29.8 μm was placed in a temperature controlled furnace with a temperature control accuracy of 0.1 °C. The size and optical damage threshold of the crystal purchased from HC Photonics Corp. were 2 mm × 4 mm × 50 mm and 200 MW/cm^2, respectively. A plane-convex lens (L) with a focal length of 1200 mm was placed between the 1064 nm EOCD-laser cavity and the OPO cavity to compress the diameter of the 1064 nm EOCD-laser to approximately 1.8 mm. This ensures that the 1064 nm EOCD-laser beam with high peak power can be compressed into the MgO: PPLN crystal while maintaining its power density below the optical damage threshold of the MgO: PPLN crystal. Furthermore, by rotating a half-wave plate (λ/2-plate), the polarization direction of the 1064 nm EOCD-laser was precisely adjusted to satisfy the quasi-phase matching condition (p → p + p) of the MgO: PPLN crystal. By using the difference frequency effect and the temperature tuning of the MgO: PPLN crystal in the range of 30 °C to 200 °C, the wavelength tunable near-infrared signal light oscillation in the OPO cavity and the mid-IR idler light output can be realized. The coatings on the surfaces of the relevant optical elements are shown in Table 1.

Based on laser cavity stability theory, significant thermal effects in the Nd: YAG and MgO: PPLN crystals often degrade beam quality and stability of the 1064 nm EOCD-laser, and can even lead to cavity detuning. This requires optimizing the cavity structures of the 1064 nm EOCD-laser and OPO to ensure thermal insensitivity in the thermal lens focal length range corresponding to the pump power of the LD arrays, i.e. each cavity remains in a stable oscillatory state. When the MgO: PPLN crystal is at a typical temperature control of 150 °C, the theoretical wavelengths of the signal light and idler light generated based on the difference frequency are 1525 nm and 3519 nm, respectively. When the LD pump current was raised from 30 to 75 A and the pulse repetition frequency was set to 1 kHz, the thermal focal lengths of the Nd: YAG and MgO: PPLN crystals, as measured using the method based on cavity stability theory [31], decreased from ~ 160 mm to ~ 90 mm and from ~ 210 mm to ~ 100 mm, respectively. At the pulse repetition frequency of 100 Hz, the thermal focal lengths of the Nd: YAG and MgO: PPLN crystals decreased from ~ 280 mm to ~ 170 mm and from ~ 330 mm to ~ 260 mm, respectively. The cavity structures of the 1064 nm EOCD-laser and OPO were optimized using the ABCD matrix theory and the laser cavity analysis and design (LASCAD) software [32]. When the LD pump current was increased from 30 to 75 A, the stability parameters (A + D)/2 of the sagittal (s) and tangential (t) beams of the 1064 nm EOCD-laser and the signal light at 1525 nm were calculated as follows:

$$1064\text{nm}-\text{pump laser}\begin{cases}@1\text{kHz}\begin{cases}\left|\frac{A_s+D_s}{2}\right|\approx 0.3874\rightarrow 0.7115\\ \left|\frac{A_t+D_t}{2}\right|\approx 0.4251\rightarrow 0.7761\end{cases}\\ @100\text{Hz}\begin{cases}\left|\frac{A_s+D_s}{2}\right|\approx 0.4755\rightarrow 0.5779\\ \left|\frac{A_t+D_t}{2}\right|\approx 0.5078\rightarrow 0.6011\end{cases}\end{cases} \quad (1)$$

$$1525\text{ nm}-\text{signal laser}\begin{cases}@1\text{kHz}\begin{cases}\left|\frac{A_s+D_s}{2}\right|\approx 0.4577\rightarrow 0.7955\\ \left|\frac{A_t+D_t}{2}\right|\approx 0.4914\rightarrow 0.8519\end{cases}\\ @100\text{Hz}\begin{cases}\left|\frac{A_s+D_s}{2}\right|\approx 0.5641\rightarrow 0.6414\\ \left|\frac{A_t+D_t}{2}\right|\approx 0.6152\rightarrow 0.6822\end{cases}\end{cases} \quad (2)$$

The above calculations show that the stability parameters (A + D)/2 of the 1064 nm EOCD-laser and the signal light at 1525 nm always satisfy the stable oscillation condition with the absolute value less than 1 [33]. Correspondingly, M_1, M_2, M_3 and M_4 were identified as plane, plane-concave, plane and plane-concave mirrors, respectively. The curvature radii of the concave surfaces for the M_2 and M_4 facing the cavity were 1 m and 500 mm, respectively. The cavity lengths of the 1064 nm EOCD-laser and OPO were ~ 229 mm and ~ 75 mm, respectively. The distances between adjacent optical elements from M_1 to M_2 were ~ 15 mm, ~ 28 mm, ~ 35 mm, ~ 12 mm, ~ 28 mm, and ~ 35 mm, respectively. The distances between adjacent optical elements from M_3 to M_4 were ~ 12 mm and ~ 13 mm, respectively.

3 BC filtering analysis

The BC was inserted after BP_1 and its transmission plane was perpendicular to the optical axis of the cavity for the 1064 nm EOCD-laser. When a half-wave voltage is applied to the TEOM-MgO: LN crystal, the p-polarized 1064 nm fundamental frequency light achieving low-loss oscillation in the cavity, will be split into ordinary (o-light) and extraordinary (e-light) light beams by the BC, which has natural birefringence. The transmittance T_p of the p-polarized

1064 nm fundamental frequency light after passing through the BC in a single round trip is as follows [10]:

$$T_p = \frac{1}{4}\left\{\left(1+(\frac{2n}{n^2+1})^4\right)\cos(\frac{1}{\Delta\varphi}) + \sqrt{\left(1+(\frac{2n}{n^2+1})^4\right)^2\cos^2(\frac{1}{\Delta\varphi}) - 4(\frac{2n}{n^2+1})^4}\right\}^2 \quad (3)$$

$$\Delta\varphi = \frac{4\pi(n_e - n_o)z}{\lambda} \quad (4)$$

where $z = 2.4$ mm and $\lambda = 1064$ nm represent the thickness of the BC and the wavelength, respectively. $n_o = 1.544$ and $n_e = 1.553$ represent the refractive indices of the o-light and the e-light in the BC at 1064 nm, respectively. $\Delta\varphi$ represents the phase delay between o-light and e-light of the p-polarized 1064 nm fundamental frequency light after passing through the BC in a single round trip.

When the optical axis of the p-polarized 1064 nm fundamental frequency light forms an angle of 45° with the optical axis of the BC, the $\Delta\varphi$ value between the p-polarized 1064 nm fundamental frequency light leaving BP_1 and the p-polarized 1064 nm fundamental frequency light returning BP_1 through BC is an integer multiple of π [29]:

$$\Delta\varphi = \pm m\pi \quad (5)$$

where m represents zero or a natural number.

The variation law of T_p with $\Delta\varphi$ obtained based on Eqs. (3)-(5) is shown in Fig. 2. When m is even or zero, the T_p is 100%. When m is odd, the T_p is only 76.3%. Therefore, only the longitudinal modes of the p-polarized 1064 nm fundamental frequency light that satisfy m being an even number or zero can achieve low-loss oscillation in the cavity. Longitudinal modes that do not meet this condition will be suppressed due to excessive reflection losses. This method reduces the number of longitudinal modes, thereby alleviating mode competition and further decreasing the peak-to-peak instability of the 1064 nm EOCD-laser used as the pump source.

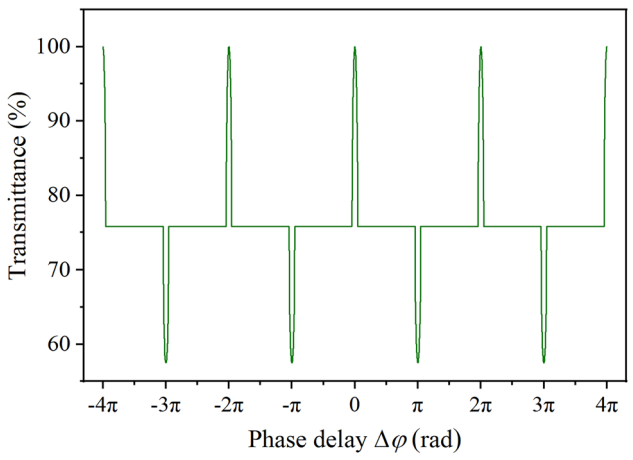

Fig. 2 Transmittance of the p-polarized 1064 nm EOCD-laser on the surface of BC with different $\Delta\varphi$ values

4 Result and discussions

4.1 Output characteristics of the 1064 nm EOCD-laser

Figure 3 and Table 2 respectively show the trends of average power, pulse width, single pulse energy, peak power, and peak-to-peak instability of pulse width and single pulse energy for 5000 pulses of the 1064 nm EOCD-laser at a 1 kHz repetition rate, as a function of LD pump current under conditions both without and with BC insertion. The single pulse energy is calculated by dividing the average power by the pulse repetition frequency, while the peak power is obtained by dividing the single pulse energy by the pulse width. Instability is defined as the difference between the maximum and minimum values of the output parameter (single pulse energy or pulse width) over a given period, divided by the arithmetic mean of that parameter [11, 29]. At the maximum pump current of 75 A, the beam quality factors M^2 and the near-field beam spot's 2D and 3D images of the 1064 nm EOCD-laser in the two aforementioned states were measured using a laser beam quality analyzer without power attenuation (ModeScan1740, Photon USA Inc., minimum response to laser pulse repetition frequency: 1 kHz), as shown in Fig. 4.

Compared to the state without BC, the insertion loss of the BC typically increases to an increase in the LD pump power threshold of the cavity. However, the output characteristics of the cavity improved with the insertion of the BC, resulting in a pulsed laser with a central wavelength of 1064.33 nm. For example, under a maximum LD pump current of 75 A, the 1064 nm EOCD laser achieved an average power of 8.16 W, a single pulse energy of 8.16 mJ, a pulse width of 6.34 ns, a peak power of 1.29 MW, and a line width of 0.24 nm. Correspondingly, the peak-to-peak instability of pulse width and single pulse energy was ± 1.24% and ± 1.53%, respectively. The M^2 factors along the X and Y axes were 4.155 and 4.359, respectively.

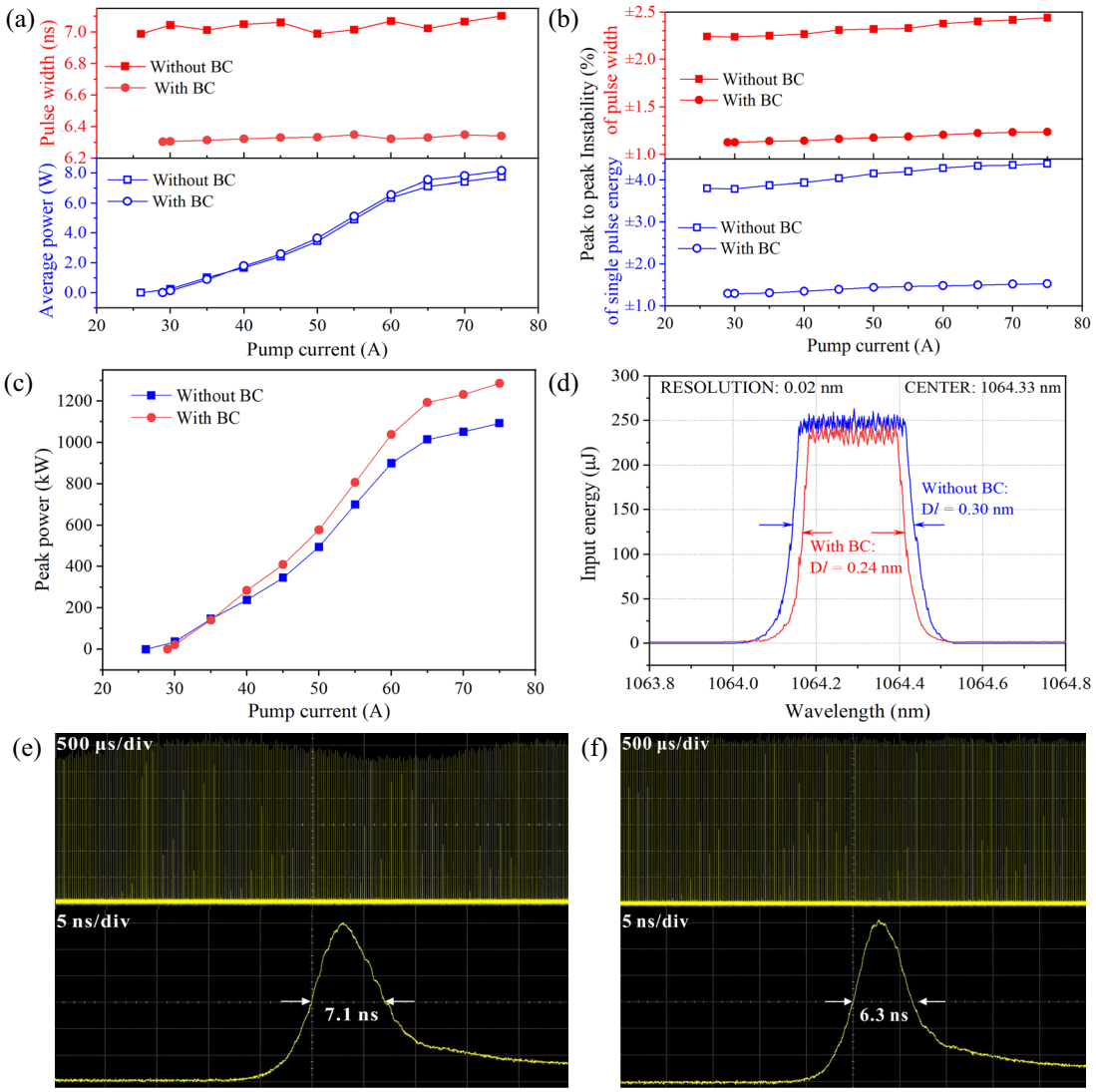

Fig. 3 Output characteristics of the 1064 nm EOCD-laser without using BC and with using BC at a pulse repetition frequency of 1 kHz. (**a**) Average output power and pulse width versus incident LD pump current; (**b**) Peak-to-peak instability of pulse width and single pulse energy versus incident LD pump current; (**c**) Peak power versus incident LD pump current; (**d**) Measured spectra; (**e**) Pulse trains recorded at different timescales of the 1064 nm EOCD-laser without BC; (**f**) Pulse trains recorded at different timescales of the 1064 nm EOCD-laser with BC

Table 2 Output parameters of the 1064 nm cavity dumped laser at the pulse repetition frequency of 1 kHz and maximum LD pump current of 75 A

With BC	Maximum average power	Maximum single pulse energy	Pulse width	Peak power	Spectral line width	Instability		M^2	
						pulse width	single pulse energy	M^2_x	M^2_y
No	7.76 W	7.76 mJ	7.1 ns	1.09 MW	0.30 nm	±2.44%	±4.38%	6.188	6.308
Yes	8.16 W	8.16 mJ	6.3 ns	1.29 MW	0.24 nm	±1.24%	±1.53%	4.155	4.359

The improvements in these laser output parameters can be credited to selective filtering facilitated by the BC. It effectively diminishes the number of longitudinal modes for the p-polarized 1064 nm EOCD-laser, enhancing beam quality and significantly alleviating mode competition in the cavity. The reduction in mode competition not only decreases the peak-to-peak instability of pulse width and single pulse energy but also further enhances the gain of

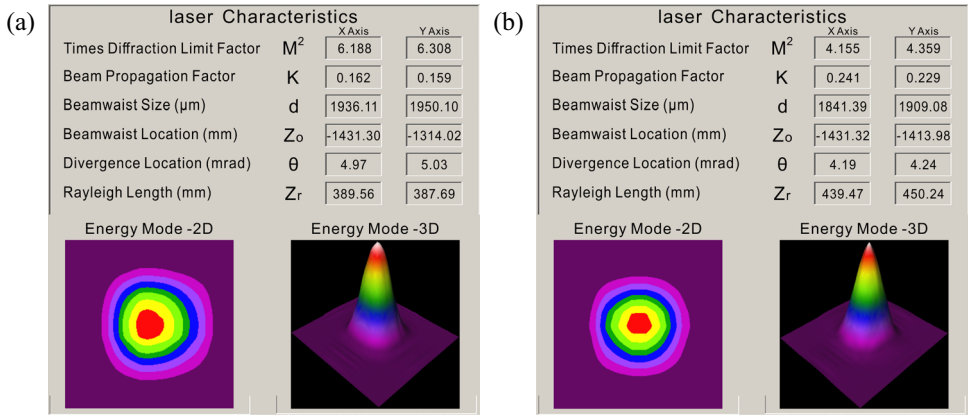

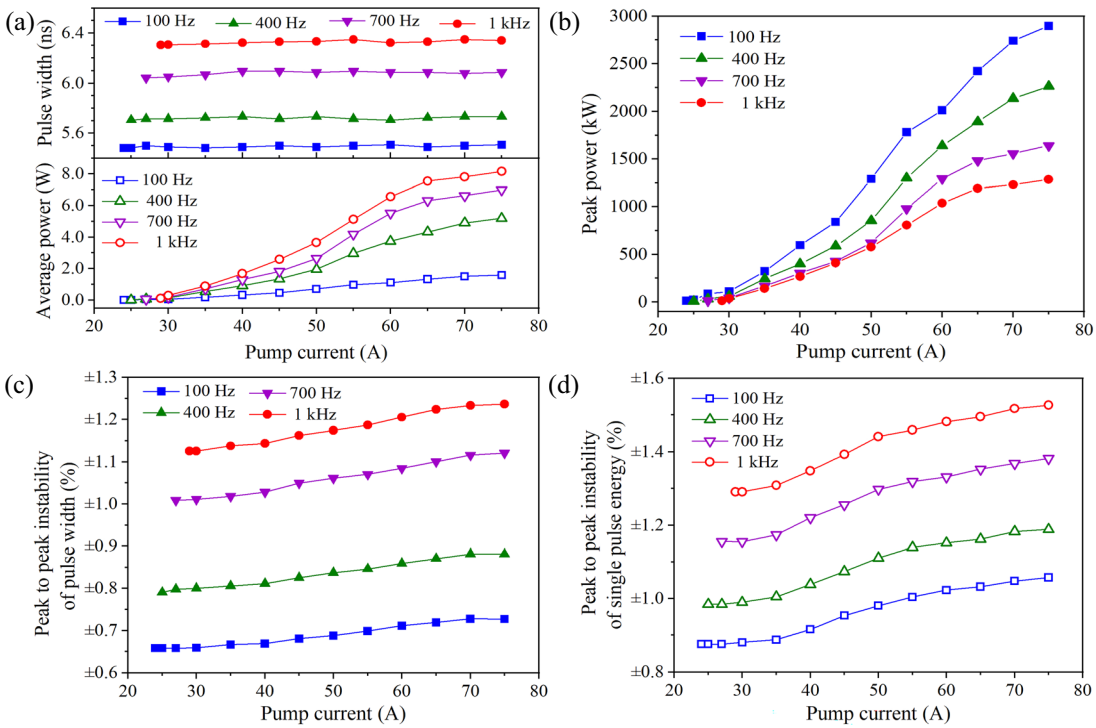

Fig. 5 Output characteristics of the 1064 nm EOCD-laser with BC under different LD pump currents and different pulse repetition frequencies. (**a**) Average output power and pulse width versus incident pump current and pulse repetition frequency; (**b**) Peak power versus incident pump current and pulse repetition frequency; (**c**) Peak-to-peak instability of pulse width versus incident pump current and pulse repetition frequency; (**d**) Peak-to-peak instability of single pulse energy versus incident pump current and pulse repetition frequency

the longitudinal modes that satisfy Eq. (5). Therefore, the use of the BC helps achieve a 1064 nm EOCD-laser with higher peak power, lower peak-to-peak instability of the pulse width and single pulse energy, and better beam quality.

The output characteristics of the 1064 nm EOCD-laser when using the BC at the maximum LD pump current of 75 A are shown in Fig. 5, Fig. 6, and Table 3. At pulse repetition frequencies of 100 Hz, 400 Hz, 700 Hz, and 1 kHz, the 1064 nm EOCD laser achieved maximum average powers of 1.59 W, 5.19 W, 6.99 W, and 8.16 W, respectively. Correspondingly, the maximum single pulse energies were 15.90 mJ, 12.98 mJ, 10.31 mJ, and 8.16 mJ. The corresponding narrowest pulse widths measured were 5.5 ns, 5.7 ns, 6.1 ns, and 6.3 ns, respectively. Additionally, the maximum peak powers reached were 2.89 MW, 2.28 MW, 1.64 MW, and 1.30 MW. The peak-to-peak instability of the pulse width and single pulse energy for the four pulse repetition frequencies were ($\xi_\tau = \pm 0.73\%$, $\xi_E = \pm 1.06\%$) at 100 Hz, ($\xi_\tau = \pm 0.88\%$, $\xi_E = \pm 1.19\%$)

at 400 Hz、($\xi_\tau = \pm 1.12\%$, $\xi_E = \pm 1.38\%$) at 700 Hz, and ($\xi_\tau = \pm 1.24\%$, $\xi_E = \pm 1.53\%$) at 1 kHz.

The results above demonstrate that the time interval between two adjacent laser pulses is significantly longer than the upper energy level lifetime of the Nd: YAG crystal at 1064 nm (~ 230 μs) in the pulse repetition frequency range from 100 Hz to 1 kHz. The adjacent laser pulses do not interfere with each other, while each pulse receives sufficient gain from the Nd: YAG crystal. This helps achieve the 1064 nm EOCD-laser with high peak power and excellent peak-to-peak stability [34]. However, the growing thermal effects in the Nd: YAG crystal detrimentally affect cavity stability, leading to a slight increase in peak-to-peak instability of pulse width and single pulse energy for the 1064 nm EOCD-laser, especially under higher LD pump current and pulse repetition frequencies.

As shown in Figs. 5a and 6, the pulse width of the 1064 nm EOCD-laser fluctuated only in a very narrow range of 5.5 ns to 6.3 ns as the pulse repetition frequency increased from 100 Hz to 1 kHz at the maximum LD pump current of 75 A. The results indicate that, while the 1064 nm EOCD laser exhibited excellent pulse width stability across diverse LD pump currents and pulse repetition frequencies, the measured pulse width slightly exceeded the transit time

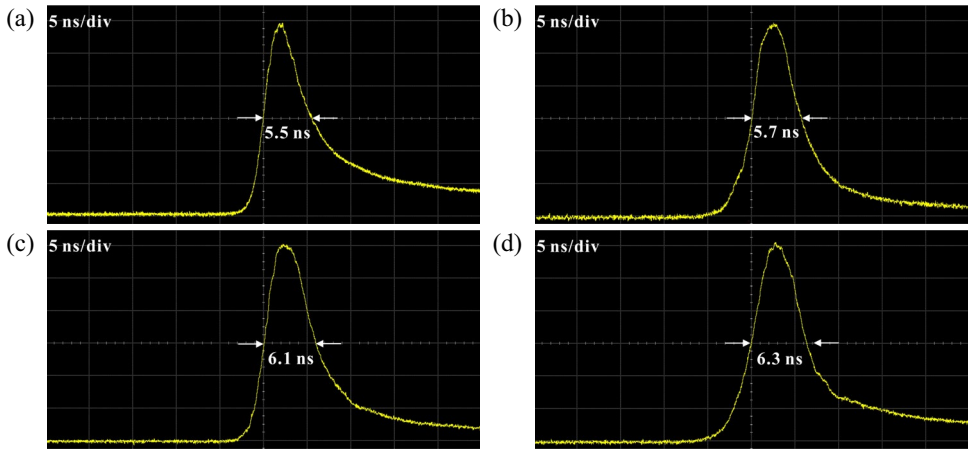

Fig. 6 Pulse profiles of the 1064 nm EOCD-laser with BC at (**a**) 100 Hz; (**b**) 400 Hz; (**c**) 700 Hz; (**d**) 1 kHz

Table 3 Output parameters of the 1064 nm EOCD-laser with BC under maximum LD pump current of 75 A

Repetition frequency	Maximum average power	Maximum single pulse energy	Pulse width	Peak power	Instability	
					pulse width	single pulse energy
100 Hz	1.59 W	15.90 mJ	5.5 ns	2.89 MW	±0.73%	±1.06%
400 Hz	5.19 W	12.98 mJ	5.7 ns	2.28 MW	±0.88%	±1.19%
700 Hz	6.99 W	9.99 mJ	6.1 ns	1.64 MW	±1.12%	±1.38%
1 kHz	8.16 W	8.16 mJ	6.3 ns	1.30 MW	±1.24%	±1.53%

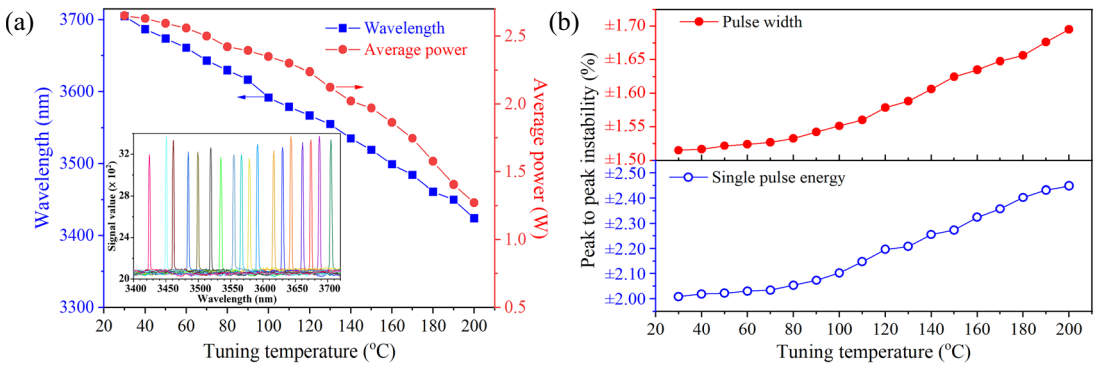

Fig. 7 Output characteristics of the idler light pumped by the 1064 nm EOCD-laser with BC at a pulse repetition frequency of 1 kHz and maximum LD pump current of 75 A. (**a**) Wavelength and average output power versus incident tuning temperature. Insets: Measured spectra; (**b**) Peak-to-peak instability versus incident tuning temperature

ρ of a photon in the cavity ($\rho = 2\ l/C \approx 2.4$ ns, l is the optical length of cavity, C is the light speed in vacuum). This discrepancy primarily occurs when the rise response time of the electro-optic switch surpasses the ρ value, leading to the pulse width being predominantly influenced by the rise response time [11].

4.2 Output characteristics of OPO pumped by the 1064 nm EOCD-laser with BC

When the tuning temperature of the MgO: PPLN crystal was elevated from 30 °C to 200 °C, the OPO produced wavelength-tunable idler light in the mid-IR range of 3705.2 nm to 3424.3 nm, exhibiting a spectral line width of ~ 3 nm and a tuning line width of ~ 281 nm (refer to Fig. 7). Simultaneously, the corresponding signal light

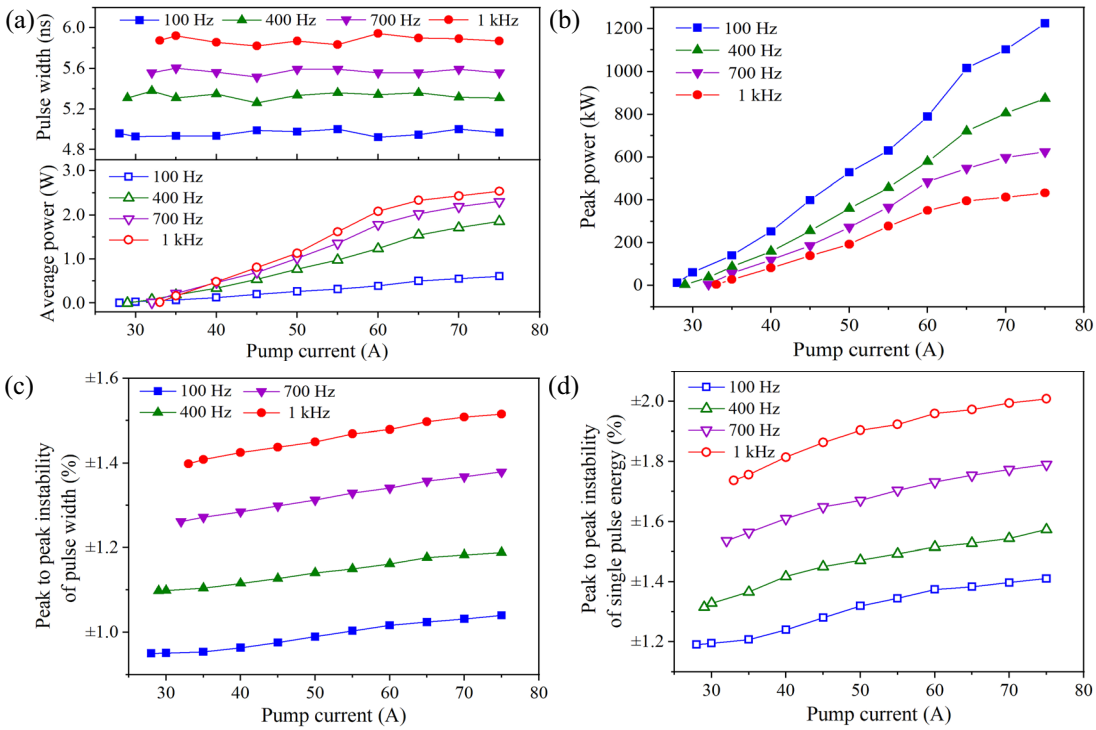

Fig. 8 Output characteristics of the idler light at 3705.2 nm pumped by the 1064 nm EOCD-laser with BC under different LD pump current and different pulse repetition frequencies. (**a**) Average output power and pulse width versus incident pump current and pulse repetition frequency; (**b**) Peak power versus incident pump current and pulse repetition frequency; (**c**) Peak-to-peak instability of pulse width versus incident pump current and pulse repetition frequency; (**d**) Peak-to-peak instability of single pulse energy versus incident pump current and pulse repetition frequency

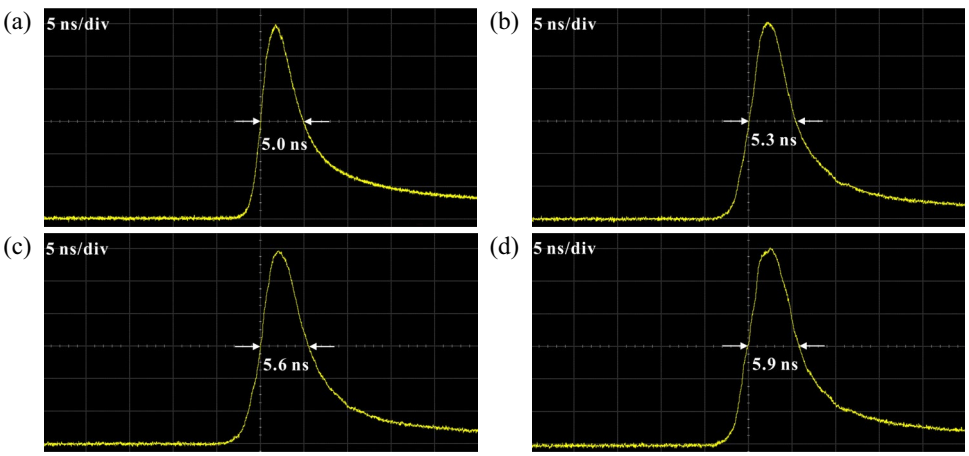

Fig. 9 Pulse profiles of the idler light at 3705.2 nm under (**a**) 100 Hz; (**b**) 400 Hz; (**c**) 700 Hz; (**d**) 1 kHz

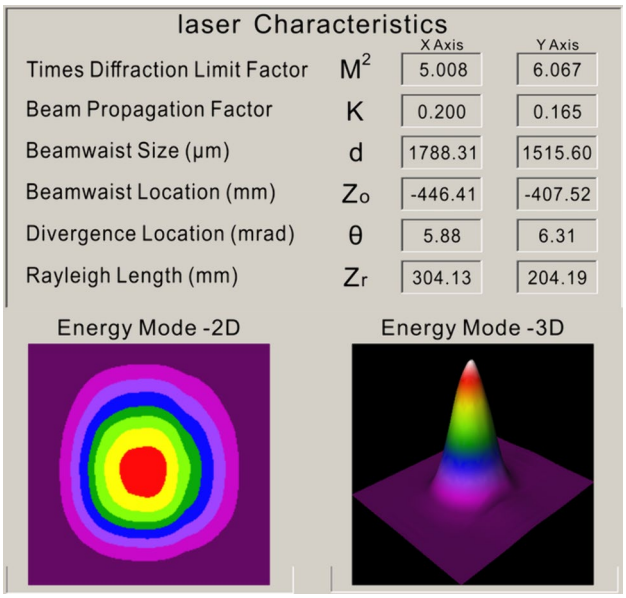

Fig. 10 Laser beam quality test data of the idler light at 3705.2 nm under a pulse repetition frequency of 1 kHz

oscillating in the OPO exhibited a wavelength tuning range of 1493.3 nm to 1544.3 nm and a tuning line width of 51.0 nm. Elevating the tuning temperature typically intensifies thermal relaxation collisions among particles in the crystal, leading to a reduction in the nonlinear frequency conversion efficiency of the MgO: PPLN crystal. Consequently, there was a trend where the maximum average output power of the idler light decreases with rising tuning temperature at the maximum LD pump current of 75 A and maximum pulse repetition frequency of 1 kHz.

As depicted in Figs. 8, 9, 10 and Table 4, the idler light with a maximum wavelength of 3705.2 nm achieved at a minimum tuning temperature of 30 °C exhibited output characteristics akin to the 1064 nm EOCD-laser. On one hand, the average power, single pulse energy, and peak power of the idler light at 3705.2 nm all showed an increasing trend with the increase in LD pump current under the same pulse repetition frequency. Correspondingly, the average power and oscillation threshold under the same LD pump current increased with the increase of the pulse repetition frequency, while the single pulse energy and peak power all decreased with the increase in the pulse repetition frequency. The pulse width of the idler light increased only from 5.0 ns to 5.9 ns as the pulse repetition frequency rose from 100 Hz to 1 kHz at the maximum LD pump current of 75 A. The above pulse width data show that the pulse width of idling light is shorter than that of 1064 nm EOCD-laser. This can be explained by the fact that the parts (at the rising and falling edges) of pulse waveform of the 1064 nm EOCD-laser with a Gaussian intensity distribution in the time domain are unable to achieve nonlinear frequency conversion due to their low intensity. On the other hand, the idler light at 3705.2 nm inherited the advantages of high peak power and low peak-to-peak instability from the 1064 nm EOCD-laser based on BC filtering. Despite being affected by adverse factors such as the peak-to-peak instability of the 1064 nm EOCD laser and thermal effects in the Nd: YAG and MgO: PPLN crystals, the pulse width and peak-to-peak stability of the idler light had marginally degraded but remain exceptionally low.

Under the conditions of a minimum tuning temperature of 30 °C and pulse repetition frequencies of 100 Hz, 400 Hz, 700 Hz, and 1 kHz, the maximum average powers of the idler light at 3705.2 nm were 0.61 W, 1.86 W, 2.31 W, and 2.54 W, respectively. The maximum optical-to-optical (1064.33 nm to 3705.2 nm) conversion efficiencies were 38.36%, 35.84%, 33.05%, and 31.13%, respectively. The corresponding narrowest pulse widths measured were 5.0 ns, 5.3 ns, 5.6 ns, and 5.9 ns, respectively. Additionally, the maximum peak powers reached were 1.22 MW, 0.88 MW, 0.59 MW, and 0.43 MW. The peak-to-peak instability of the pulse width and single pulse energy for the four pulse repetition frequencies were ($\xi_\tau = \pm 1.04\%$, $\xi_E = \pm 1.41\%$) at 100 Hz, ($\xi_\tau = \pm 1.19\%$, $\xi_E = \pm 1.57\%$) at 400 Hz、($\xi_\tau = \pm 1.38\%$, $\xi_E = \pm 1.79\%$) at 700 Hz, and ($\xi_\tau = \pm 1.52\%$, $\xi_E = \pm 2.01\%$) at 1 kHz. Furthermore, the M^2 factors at a maximum pulse repetition frequency of 1 kHz were measured to be $M^2_x = 5.008$ and $M^2_y = 6.067$.

Table 4 Output parameters of the idler light at 3705.2 nm under the tuning temperature of 30 °C and maximum LD pump current of 75 A

Repetition frequency	Maximum average power	Maximum single pulse energy	Pulse width	Peak power	Instability	
					pulse width	single pulse energy
100 Hz	0.61 W	6.10 mJ	5.0 ns	1.22 MW	±1.04%	±1.41%
400 Hz	1.86 W	4.65 mJ	5.3 ns	0.88 MW	±1.19%	±1.57%
700 Hz	2.31 W	3.33 mJ	5.6 ns	0.59 MW	±1.38%	±1.79%
1 kHz	2.54 W	2.54 mJ	5.9 ns	0.43 MW	±1.52%	±2.01%

5 Conclusion

In conclusion, we introduced a mid-IR OPO using an MgO: PPLN crystal with a polarization period of 29.8 μm, which was pumped by a 1064 nm EOCD-laser. In the temperature tuning range of the MgO: PPLN crystal from 30 oC to 200 °C, a wavelength tunable mid-IR idler light with high peak power, low peak-to-peak instability of pulse width and single pulse energy, a wavelength tuning range of 3705.2 nm to 3424.3 nm, and a pulse repetition frequency tuning range of 100 Hz—1 kHz was achieved. At the combined conditions of a minimum tuning temperature of 30 °C, a maximum pulse repetition frequency of 1 kHz, and a maximum LD pump current of 75 A, the idler light at 3705.2 nm with a maximum average output power of 2.54 W was obtained, corresponding to an optical-to-optical (1064.33 nm to 3705.2 nm) conversion efficiency of 31.13%. At the pulse repetition frequency of 100 Hz, the idler light at 3705.2 nm with a maximum single pulse energy of 6.10 mJ, narrowest pulse width of 5.0 ns, a maximum peak power of 1.22 MW, a minimum peak-to-peak instability of ± 1.04% for the pulse width, a minimum peak-to-peak instability of ± 1.41% for the single pulse energy, and a maximum optical-to-optical conversion efficiency of 38.36% was achieved. The research results demonstrate that BC filtering can effectively reduce the number of longitudinal modes of the 1064 nm all-solid-state pulsed laser based on electro-optic cavity-dumping and alleviate mode competition among these longitudinal modes. This improvement enhances the peak power, peak-to-peak stability of pulse width and single pulse energy for the mid-IR OPO when the 1064 nm all-solid-state pulsed laser incorporating electro-optic cavity-dumping and BC filtering is used as the pump source. Our research findings provide a valuable reference for manufacturing high-quality wavelength tunable mid-IR pulsed laser sources with high peak power and low peak-to-peak instability in fields such as atmospheric remote sensing, environmental monitoring, laser radar, and optoelectronic countermeasures.

Acknowledgements The authors would like to acknowledge both the Open Project of Key Laboratory of Metrological Optics and Application for State Market Regulation of China (No. SXJL2023001KF) and the Shaanxi Key Science and Technology Innovation Team Project of China (No. 2023-CX-TD-06) for funding provided towards the OPOs project.

Author contributions Conceptualization: YB. ethodology: YB. Validation: All authors. Formal analysis: All authors. Investigation:GZW, SYY, WRD. Resources: YB, BLL. Data Curation: GZW, YL,XYZ. Writ-ing-Original Draft: GZW. Writing-Review & Editing: All authors. Visualization: GZW, XYZ. Supervision: YB. Project administration:YB, BLL. Funding acquisition: YB, BLL.

Data availability Data underlying the results presented in this paper are not publicly available at this time but may be obtained from the authors upon reasonable request.

Declarations

Conflict of interest The authors declare no competing interests.

References

1. M.A. Medina, M. Piotrowski, M. Schellhorn, F.R. Wagner, A. Berrou, A. Hildenbrand-Dhollande, Beam quality and efficiency of ns-pulsed high-power mid-IR ZGP OPOs compared in linear and non-planar ring resonators. Opt. Express **29**(14), 21727–21737 (2021). https://doi.org/10.1364/OE.430717
2. S. Parsa, S.C. Kumar, B. Nandy, M. Ebrahim-Zadeh, Yb-fiber-pumped, high-beam-quality, idler-resonant mid-infrared picosecond optical parametric oscillator. Opt. Express **27**(18), 25436–25444 (2019). https://doi.org/10.1364/OE.27.025436
3. M. Schellhorn, G. Spindler, M. Eichhorn, Mid-infrared ZGP OPO with divergence compensation and high beam quality. Opt. Express **26**(2), 1402–1410 (2018). https://doi.org/10.1364/OE.26.001402
4. T.T. Zhou, Y. He, L.L. Yang, N. Li, J. Huang, D.Y. Liu, Y.Y. Gou, L.L. Miao, C.J. Zhao, Efficient and wavelength-tunable mid-infrared fluoride fiber laser modulated by Cs_xWO_3 nanocrystals. Infrared Phys. Technol. **137**, 1350–4495 (2024). https://doi.org/10.1016/j.infrared.2024.105192
5. Q.Y. Lu, S. Slivken, D.H. Wu, M. Razeghi, High power continuous wave operation of single mode quantum cascade lasers up to 5 W spanning lambda similar to 3.8–8.3 μm. Opt. Express **28**(10), 15181–15188 (2020). https://doi.org/10.1364/OE.393069
6. Z.H. Wang, B. Zhang, J. Liu, Y.F. Song, H. Zhang, Recent developments in mid-infrared fiber lasers: Status and challenges. Opt. Laser Technol. **132**, 106497 (2020). https://doi.org/10.1016/j.optlastec.2020.106497
7. Y.C. Zhang, Y.M. Duan, Z.G. Wang, D. Zhang, J. Zhang, Y.J. Zhang, H.Y. Zhu, Continuous-wave widely tunable MgO: PPLN optical parametric oscillator with compact linear cavity. IEEE Photon. **30**(20), 1756–1759 (2018). https://doi.org/10.1109/LPT.2018.2868736
8. F. Liégeois, C. Vercambre, Y. Hernandez, M. Salhi, D. Giannone, Pulsed high-peak-power and single-frequency fiber laser design for LIDAR aircraft safety application. SPIE 6367, 63670H-1–63670H-10 (2006). https://doi.org/10.1117/12.688203
9. G. Canat, B. Augère, C. Besson, A. Dolfi-Bouteyre, A. Durécu, D. Goular, J. Le Gouët, L. Lombard, C. Planchat, M. Valla, High peak power single-frequency mopfa for lidar applications. in Conference on Lasers and Electro-Optics, paper AM3K.4. (2016). https://doi.org/10.1364/CLEO_AT.2016.AM3K.4
10. J.L. Yan, B. Li, G.Z. Wang, S.Y. Yang, B.L. Lu, Y. Bai, High stability and low noise laser-diode end-pumped Nd: YAG ceramic passively Q-switched laser at 1123 nm based on a $Ti_3C_2T_x$-PVA saturable absorber. Chin. Phys. B **32**(11), 114212 (2023). https://doi.org/10.1088/1674-1056/acf495
11. Y. Bai, B. Bai, D. Li, Y.X. Sun, J.L. Li, L. Hou, M.X. Hu, J.T. Bai, Pulsed LD side-pumped MgO: LN electro-optic cavity-dumped 1123 nm Nd: YAG laser with short pulse width and high peak power. High Power Laser Sci. Eng. **6**, e4 (2018). https://doi.org/10.1017/hpl.2017.38
12. H.J. Jiang, J.C. Lai, W. Yan, C.Y. Wang, Z.H. Li, Theoretical distribution of range data obtained by laser radar and its applications. Opt. Laser Technol. **45**, 278–284 (2013). https://doi.org/10.1016/j.optlastec.2012.06.035
13. J. Yun, C.X. Gao, S.L. Zhu, C.D. Sun, H.D. He, L. Feng, L.J. Dong, L.Q. Niu, High-peak-power, single-mode, nanosecond pulsed, all-fiber laser for high resolution 3D imaging LIDAR

system. Chin. Opt. Lett. **10**(12), 39–41 (2012). https://doi.org/10.3788/COL201210.121402
14. B. Cole, L. Goldberg, S. Chinn, L.A. Pomeranz, K.T. Zawilski, P.G. Schunemann, J. McCarthy, Compact and efficient mid-IR OPO source pumped by a passively Q-switched Tm: YAP laser. Opt. Lett. **43**(5), 1099–1102 (2018). https://doi.org/10.1364/OL.43.001099
15. Z. Lv, Y. Shen, Y. Wen, E.P. Wang, Z.M. Wang, W.L. Li, Y. Bo, Q.J. Peng, High power widely tunable mid-IR (5–7.2 μm) ZnGeP2 optical parametric oscillator pumped by a 2.09 μm laser. Infrared Phys. Technol. **134**, 104879 (2023). https://doi.org/10.1016/j.infrared.2023.104879
16. X. Wei, S. Zhang, Z. Liu, X. Ye, W. Yin, H. Ren, B. Kang, Z. Yuan, W. Wang, Y. Ma, High-power mid-infrared ZGP optical parametric oscillator directly pumped by pulsed Tm: YLF laser at 1908 nm. Opt. Laser Technol. **161**, 109135 (2023). https://doi.org/10.1016/j.optlastec.2023.109135
17. J. Mei, H. Yang, S. He, Self Q-switched single-frequency all-fiber laser. Appl. Opt. **63**(12), 3168–3173 (2024). https://doi.org/10.1364/AO.519130
18. W.W. Li, J.H. Zou, Y.Z. Huang, K.J. Wang, T.J. Du, S.S. Jiang, Z.Q. Luo, 212-kHz-linewidth, transform-limited pulses from a single-frequency Q-switched fiber laser based on a few-layer Bi_2Se_3 saturable absorber. Photonics Res. **6**(10), C29–C35 (2018). https://doi.org/10.1364/PRJ.6.000C29
19. F. Valerian, F. Eric, Femtosecond OPO pumped by a high power ytterbium rod-type fiber laser mode locked at harmonic repetition rates. Opt. Laser Technol. **148**, 107750 (2022). https://doi.org/10.1016/j.optlastec.2021.107750
20. Y. Han, Y.B. Guo, B. Gao, C.Y. Ma, R.H. Zhang, H. Zhang, Generation, optimization, and application of ultrashort femtosecond pulse in mode-locked fiber lasers. Prog. Quantum Electron. **71**, 100264 (2020). https://doi.org/10.1016/j.pquantelec.2020.100264
21. Y.X. Liu, G. Zhang, F.T. Gao, Z.Y. Jiao, D.L. Li, Passively Q-switched mode-locked laser based on a $MoS_2/MoSe_2$ heterostructure saturable absorber. Opt. Mater. **133**, 112864 (2022). https://doi.org/10.1016/j.optmat.2022.112864
22. J.H. Li, D.S. Wei, B.Q. Yao, S.Y. Mi, K. Yang, J.W. Tang, T.Y. Dai, X.M. Duan, Y.L. Ju, 43 W, 7 ns constant pulse duration, high-repetition-rate langasite cavity-dumped Ho: YAG laser and its appilcation in mid-infrared ZGP OPOs. Opt. Laser Technol. **157**, 108631 (2023). https://doi.org/10.1016/j.optlastec.2022.108631
23. J. Guo, B. Zhang, G. He, High-repetition-rate and high-peak-power sub-nanosecond 1064 nm electro-optic Q-switched laser. IEEE Photon. **33**(14), 731–734 (2021). https://doi.org/10.1109/LPT.2021.3085903
24. H. Wang, Z.Y. Li, H. Li, Z.Z. Xie, J.T. Tian, L.L. Zhao, L.M. Hu, R.Q. Tan, An electro-optic Q-switched Ho: YLF oscillator with adjustable pulse width. Infrared Phys. Technol. **138**, 105213 (2024). https://doi.org/10.1016/j.infrared.2024.105213
25. W.T. Wu, X.D. Li, R.P. Yan, Y.P. Zhou, Y.F. Ma, R.W. Fan, Z.W. Dong, D.Y. Chen, 100 kHz, 3.1 ns, 1.89 J cavity-dumped burst-mode Nd: YAG MOPA laser. Opt. Exp. **25**, 26875–26884 (2017). https://doi.org/10.1364/OE.25.026875
26. L.J. He, K. Liu, Y. Bo, X.J. Wang, J. Yang, Z. Liu, Q.S. Zong, Q.J. Peng, D.F. Cui, Z.Y. Xu, Widely-duration-tunable nanosecond pulse Nd: YVO_4 laser based on double Pockels cells. Laser Phys. Lett. **15**(5), 055004 (2018). https://doi.org/10.1088/1612-202X/aab12d
27. O. Musset, A. Petitjean, Electro-optic solution to overcome the transient regime of a cavity dumped UV laser source. Optics Commun. **551**, 130027 (2024). https://doi.org/10.1016/j.optcom.2023.130027
28. Y. Bai, Z.H. Chen, B. Li, S.Y. Yang, H. Liu, J.F. Zhou, Wavelength-variable low-noise all-solid-state yellow-green laser based on BP-frequency selection and BC-filtering. Laser Phys. **32**(12), 125803 (2022). https://doi.org/10.1088/1555-6611/aca029
29. G.Z. Wang, Y. Bai, Y. Li, J.L. Yan, S.Y. Yang, B.L. Lu, H. Zhang, A high stability and low noise passively Q-switched yellow-green laser with a $Ti_3C_2T_x$-PVA saturable absorber. Opt. Commun. **560**, 0030–4018 (2024). https://doi.org/10.1016/j.optcom.2024.130473
30. B. Bai, Y. Bai, D. Li, Y.X. Sun, J.L. Li, J.T. Bai, Double Q-switched 946 nm laser with MgO: LN electro-optic crystal and $MoSe_2$ saturable absorber. Chin. Opt. Lett. **16**(3), 031402 (2018). https://doi.org/10.3788/COL201816.031402
31. J.H. Liu, J.R. Lu, J.H. Lü, Z.S. Shao, M.H. Jiang, Thermal lens determination of end-pumped solid-state lasers by a simple direct approach. Chin. Phys. Lett. **16**(3), 181–183 (1999). https://doi.org/10.1088/0256-307X/16/3/010
32. B.H. Su, J.W. Xue, L. Sun, H.Y. Zhao, X.D. Pei, Generalised ABCD matrix treatment for laser resonators and beam propagation. Opt. Laser Technol. **43**(7), 1318–1320 (2011). https://doi.org/10.1016/j.optlastec.2011.03.031
33. Y.X. Sun, Y. Bai, D. Li, L. Hou, B. Bai, Y.Z. Gong, L.L. Yu, J.T. Bai, 946 nm Nd: YAG double Q-switched laser based on monolayer WSe2 saturable absorber. Opt. Express **25**, 21037–21048 (2017). https://doi.org/10.1364/OE.25.021037
34. Y. Orii, K. Yoshii, K. Kohno, H. Tanaka, K. Shibuya, G. Okada, Y. Mori, J. Nishimae, M. Yoshimura, High-power deep-ultraviolet light generation at 266 nm from frequency quadrupling of a picosecond pulsed 1064 nm laser with a Nd: YVO_4 amplifier pumped by a 914 nm laser diode. Opt. Express **31**(9), 14705–14714 (2023). https://doi.org/10.1364/OE.488747